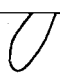


AN ABSTRACT OF THE THESIS OF

Scott A. Rutschman for the degree of Master of Science in Mechanical Engineering presented on June 12, 2003.

Title: Quantitative Comparison of Full Field Strains Experimentally Measured and Analytically Predicted for Aluminum Foams

~~Abstract/Approved~~
Redacted for privacy

Brian K. Bay 

Metallic foams have become widely available and have unique properties that make them attractive for use in a variety of engineering applications. Due to their complex structure, the behavior of foams under complex loading conditions is a subject of continued research.

Digital volume correlation is a technique wherein full-field strains in three dimensions can be measured from high resolution x-ray CT image data. This technique was employed to measured strains in two commercially available aluminum foams, one each of open and closed-cell morphology, under two complex loading scenarios: rigid spherical indentation, and uniaxial compression of a sample with a central hole. In addition to comparing the behavior of the two foams, results are also compared to strain fields analytically predicted by a third-party constitutive model implemented in finite element analysis.

Under indentation loading, the two examined foams showed a distinct difference in deformation and strain field, however the foams behaved similarly under uniaxial compression of rectangular samples with central holes. The constitutive model was found to be unsuitable for modeling the experimentally measured foams.

Quantitative Comparison of Full Field Strains Experimentally Measured and Analytically
Predicted for Aluminum Foams

by
Scott A. Rutschman

A THESIS

submitted to

Oregon State University

in partial fulfillment of
the requirements for the
degree of

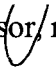
Master of Science

Presented June 12, 2003
Commencement June 2004

Master of Science thesis of Scott A. Rutschman
Presented on June 12, 2003

APPROVED:

Redacted for privacy

Major Professor  representing Redacted for privacy

Redacted for privacy


•

Redacted for privacy

 Dean of the Graduate School

I understand that my thesis will become part of the permanent collection of Oregon State University libraries. My signature below authorizes release of my thesis to any reader upon request.

Redacted for privacy

 Scott A. Rutschman, Author

ACKNOWLEDGEMENTS

The author wishes to thank the following:

- Dr. Brian Bay for providing me with the opportunity to work on this project, the funding, and for his continued advising and assistance
- The department of mechanical engineering for providing funding throughout my graduate education
- Dr. Ronald Miller for providing the constitutive model and modeling advice
- Dr. Timothy Kennedy for his assistance in implementing the constitutive model
- Fellow graduate students Dan Berry, Henri Saucy, and Sean Moran for their advice throughout this project
- My parents, Frank and Nellie Rutschman, Rebecca Johnston, and all the others who supported me throughout my graduate education

TABLE OF CONTENTS

| | <u>Page</u> |
|--|-------------|
| BACKGROUND..... | 2 |
| Manufacture | 2 |
| Structural Applications..... | 4 |
| Literature Review..... | 6 |
| Motivation | 10 |
| Strain Measurement Using Digital Volume Correlation..... | 10 |
| EXPERIMENTAL METHODS..... | 13 |
| Equipment | 13 |
| Experiments..... | 15 |
| Indention | 16 |
| Compression with Central Hole | 17 |
| Repeat Unloads | 18 |
| Data Processing..... | 18 |
| ANALYTICAL METHODS..... | 20 |
| Compression of dense metal with central hole..... | 20 |
| Constitutive Modeling..... | 20 |
| RESULTS | 22 |
| Experimental | 22 |
| Indention | 23 |
| Compression with Central Hole | 26 |
| Repeat Unloads | 30 |
| Analytical Models | 31 |

TABLE OF CONTENTS (Continued)

| | <u>Page</u> |
|--|-------------|
| Constitutive Modeling..... | 32 |
| DISCUSSION | 34 |
| Indentation..... | 34 |
| Compression with Central Hole | 35 |
| Repeat Unloads | 36 |
| Constitutive Modeling..... | 37 |
| Future Work | 39 |
| CONCLUSIONS..... | 39 |
| BIBLIOGRAPHY | 41 |
| APPENDICES..... | 43 |
| Appendix A: Data Processing and Analysis Procedure | 44 |
| Appendix B: Sample input files | 46 |

LIST OF FIGURES

| <u>Figure</u> | <u>Page</u> |
|--|-------------|
| 1. Typical stress-strain curve for an aluminum foam ⁴ | 5 |
| 2. X-ray CT system | 14 |
| 3. a) Duocel (fine) indentation b) Alporas indentation c) Duocel (coarse) with hole d) Alporas with hole | 15 |
| 4. Minimum principal strains on a diametrical plane in Duocel (fine) foam under indentation loading with corresponding renderings | 24 |
| 5. Minimum principal strains on a diametrical plane in Alporas foam under indentation loading with corresponding renderings | 25 |
| 6. Comparison of strain field depth between Alporas and Duocel (fine)..... | 26 |
| 7. Approximate planes of initial (left) and secondary (right) failure in Duocel (coarse) foam..... | 27 |
| 8. Minimum principal strains in Duocel (coarse) foam under uniaxial compressive loading with corresponding renderings | 28 |
| 9. Minimum principal strains in Alporas foam under uniaxial compressive loading with corresponding renderings | 29 |
| 10. Minimum principal strain distribution in Duocel (fine) repeat unload experiment ... | 30 |
| 11. Minimum principal strain distribution in Duocel (Coarse)..... | 30 |
| 12. Minimum principal strain distribution in Alporas..... | 31 |
| 13. Minimum principal strains in a dense metal finite element model | 32 |
| 14. Minimum principal strain in axisymmetric indentation model..... | 33 |

LIST OF TABLES

| <u>Table</u> | <u>Page</u> |
|--|-------------|
| 1. Properties of commercially available aluminum foams | 4 |
| 2. Indention experiment parameters | 16 |
| 3. Compression with central hole experiment parameters | 17 |
| 4. Parameters supplied to UMAT subroutine | 22 |
| 5. Representative minimum principal strain values from repeat unload experiments ... | 31 |
| 6. Results of Constitutive Model Trials | 32 |

**Quantitative Comparison of Full Field Strains Experimentally Measured
and Analytically Predicted for Aluminum Foams**

BACKGROUND

Metallic foams have become widely available and have unique properties that make them attractive for use in a variety of engineering applications. Due to their complex structure, the behavior of foams under complex loading conditions is a subject of continued research.

Manufacture

Aluminum foams can be divided into two distinct types: open-cell and closed-cell. Within these groups exist a wide variety of pore sizes, densities and cell structures. The specific morphology of a particular foam is greatly dependent on manufacturing techniques. Several techniques have been developed although only three methods for open-cell foam manufacture and one method for closed-cell have found use in mass production, and only these technologies will be outlined here.

Closed-cell foams are typically manufactured by 1) gas bubbling, 2) powder foaming, or 3) powder compact melting. The gas bubbling technique, which is employed by CYMAT (Ontario, Canada) is achieved by injecting gas into liquid aluminum causing a foam to form and rise to the surface of the melt where it is mechanically drawn out of the solution. In order to reduce drainage for a sufficient time such that the foam can maintain its shape through solidification, the viscosity of the aluminum melt must be increased. This is achieved by the addition of silicon carbide, aluminum oxide or magnesium oxide (5-15 wt%) to the melt.¹

The second common manufacturing technique for closed-cell foams utilizes the addition of gas-releasing particles (blowing agents) into the aluminum melt. This

technique is commercially used by Shinko Wire Company (Amagasaki City, Japan) in³ the production of "Alporas." As in the gas bubbling technique, the viscosity of the molten aluminum is increased but this time by the addition of 1.5 wt% Ca particles. Next 1.6 wt% of TiH_2 particles, which serve as the blowing agents, are added to the melt which is rapidly mixed.² The blowing agents react forming hydrogen gas which bubbles throughout the mixture. This reaction takes place in a closed vessel under constant pressure. Upon cooling the solidified foam is removed from the rectangular vessel. This process produces the most homogenous closed cell foams commercially available.¹

A third method for manufacturing closed cell aluminum foams, known as powder compact melting, relies on the same basic principle as the liquid foaming with blowing agents. However in this technique, aluminum powder and blowing agents are mixed in the solid state at room temperature. This mixture is then compacted into the desired shape, most commonly a cylinder or sheet and then heated to a temperature near the melting point of aluminum causing the blowing agents, which are ideally uniformly mixed throughout the aluminum matrix, to expand forming cells throughout the aluminum. Foams sold under the trade name "Alulight" (Ranshofen, Austria) are manufactured in this manner. This technique is also used in the manufacture of sandwich panels where the powder foam compact material is rolled into sheet form and then aluminum sheets are roll-clad to each side and then heated to expand the central foam core.

Availability of open-cell foams is limited. The most successful commercial product is "Duocel" manufactured by ERG Aerospace of California. ERG uses an investment casting method with a polymer foam as the template. In their process, an

open-cell polymer foam is filled with a ceramic slurry and cured. The mold is heated to flush the polymer out and the resulting voids are filled with molten aluminum. Heating of the mould and pressure control are required to assure that the molten aluminum completely infiltrates the voids. Lastly the casting mold is removed yielding open-celled aluminum foam. These foams are highly homogeneous but their cost is significantly higher than that of closed-cell foams.¹

The various processing methods outlined above yield a range of morphological characteristics (**Table 1**).

Table 1: Properties of commercially available aluminum foams

| Manufacturing Method | Gas Bubbling | Powder Foaming | Powder Compacting | Investment Casting |
|-----------------------------|--------------|----------------|-------------------|--------------------|
| Data Reference | 1 | 1 | 1 | 3 |
| Commercial Product | CYMAT | Alporas | Alulight | Duocel |
| Porosity (%) | 80 - 98 | 90 - 92 | 60 - 90 | 88 - 97 |
| Pore Size (mm) | 3 - 25 | 2 - 10 | Not Available | 0.5 - 4 |

Structural Applications

Aluminum foams exhibit a higher strength and stiffness than polymer foams.⁶ This has allowed for aluminum foams to replace polymer foams in some applications and has also made new applications possible. The primary properties of aluminum foams that make them attractive for a variety of structural applications are high mechanical energy absorption, high strength-to-weight ratio, and high absorption of thermal and acoustic energy. The most exploited of these characteristics to date has been the energy absorbing capacity for increasing crash safety in trains and automobiles.

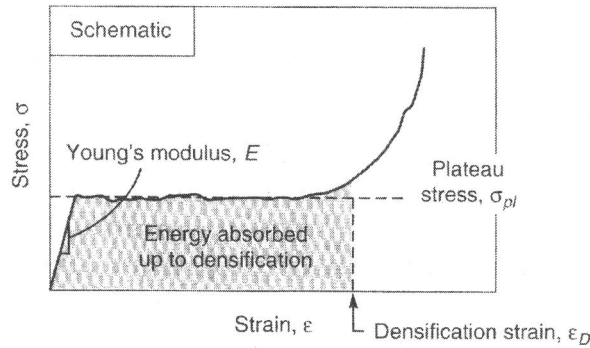


Figure 1: Typical stress-strain curve for an aluminum foam⁴

Aluminum foams exhibit an unusually long plastic strain plateau allowing for significant energy absorption (**Figure 1**). The use of aluminum foam in crash boxes (most simply blocks of foam placed behind the bumpers of automobiles and trains) has been investigated. It has been shown that such designs absorb more energy than conventional hollow-sectioned crash boxes and also localize damage thus reducing repair costs⁴. This technology has also been implemented in Japan where 2.3 m³ blocks of Alporas foam have been fitted to the fronts of trains in order to increase crash safety.¹

Although the high strength-to-weight ratio of aluminum foams makes them attractive for many structural applications, this area has yet to see the development that has occurred in the area of crash protection. This may be partially due to the established use of honeycomb structures, which exhibit properties superior to those of foam structures in this particular realm.¹ One advantage of foam over honeycombs is that it may be simpler to manufacture complex three-dimensional structures from foam rather than honeycomb materials. Automotive part manufacturer Karmann GmbH of Germany has experimented with manufacturing automotive body panels out of aluminum foams as a replacement for traditional stamped steel panels. They claim that such panels exhibit a

higher stiffness and are as much as 50% lighter than identical panels made from steel.

Furthermore, they believe use of foam panels could lead to a weight savings of up to 60kg on a compact family sedan thus improving the fuel consumption by up to 2.6 miles per gallon.⁴

Aluminum foams have also found application as sound dampening materials, most notably in traffic tunnels and under overpasses. Traditionally polymer foams are used for sound dampening, and their acoustic absorption properties are superior to those of aluminum⁴. However, aluminum foams are advantageous in that they are more durable and fire-resistant than polymer foams and they do not create harmful fumes when fires do occur. Another application which takes advantage of dampening is the use of aluminum foam as a support for mirrors in optical telescopes. Both Lockheed Missile and Space Company and the Hughes Aircraft Company Laser Systems Division have used Duocel foam in this application.⁴

It should be noted that a variety of non-structural applications have been developed for open-cell foams such as Duocel. These applications, sometimes termed "functional" applications, utilize fluid flow through the pores of open-celled foams. Some common applications are heat-exchangers and supports for reaction catalysts. The primary focus of this work is to examine the structural behavior of aluminum foam and consequently "functional" applications will not be discussed at length.

Literature Review

A significant body of work has been established regarding both the experimental measurement of various mechanical properties and the development of constitutive

models for aluminum foams. Before discussing the literature, it is beneficial to discuss the context in which this research is being carried out.

In modeling aluminum foams it is possible to consider two distinct cases: a complex geometric microstructural model utilizing a simple aluminum material model, or a simple geometric model of the same shape, such as a cube or cylinder, incorporating a more complex material model that accounts for microstructure and base material effects. Although the geometrically complex approach is attractive in that aluminum is a material that is well understood, the geometric modeling involved is very cumbersome, requires a case-by-case approach to each application of aluminum foams, and will likely never be practical for consumer use. Conversely, a geometrically simple model where aluminum foam is considered to be a continuum material is attractive for its geometric modeling simplicity and is most practical for eventual use as a common design tool, but requires a complete understanding of the pseudo-continuum material behavior of aluminum foam. It is in the direction of the continuum approach that research has focused and research in this area will be outlined here.

Perhaps the most important issue when considering aluminum foam as a continuum material is to establish the minimum size scale which can be considered in order to assure continuum behavior. An accepted range of 6-8 cell widths has been established by E.W. Andrews *et al.*⁵ and is widely accepted. Specifically, all relevant linear dimensions in an experiment (e.g. sample size, hole size, indenter size) should be at least 6-8 times a typical cell size.

Theory regarding the behavior of cellular solids was developed by Gibson and Ashby primarily from modeling and experimental testing of polymer foams⁶. These

theories have translated well to aluminum foams. They present an extensive series of relationships relating the properties of foams to the base material from which they are composed and their relative densities.⁴ The general form of these relationships is shown (**Equation 1**) where the subscript "s" denotes a property of the solid, the superscript "*" denotes a property of the foam, ρ denotes density and α and n are constants. Equations of this form have served as theoretical comparison for experimental work and as a basic design aid for prediction of foam behavior.

$$\frac{P^*}{P_s} = \alpha \left\{ \frac{\rho^*}{\rho_s} \right\}^n \quad [1]$$

The uniaxial stress-strain curve for aluminum foams in both tension and compression has been well established.⁷⁻¹¹ These tests have provided the basic material properties such as Young's modulus, yield strength, Poisson's ratio, and anisotropy. These tests have also revealed some unique characteristics of aluminum foams. For example, localized cell yielding at small loads distorts the initial loading modulus values so unloading modulus values are typically reported.^{8,11} Also, most foams exhibit transversely isotropic behavior¹⁰ as a result of elongated cells in a single direction due to gravity or mechanical extraction during the manufacturing process. The most significant result, from a modeling perspective, is the Poisson expansion of foams. In the elastic realm aluminum foam behavior is very similar to that of dense metals ($\nu \approx 0.3$),⁴ but whereas dense metals undergo no volumetric change in the plastic realm, foams are highly compressible ($\nu < 0.1$).¹² As a consequence of this result, foams are capable of yielding under hydrostatic loads and a parameter called the Plastic Poisson's Ratio is

frequently measured in order to develop yield criteria for foams.^{13,14} Biaxial and hydrostatic tests have been used to investigate the yield surface of aluminum foams and this research has also contributed to the development of constitutive models.^{12,14}

The modes of deformation in metallic foams are a subject of continued interest. Observation and characterization of deformation under both uniaxial and biaxial loads using optical imaging,^{8,15,16} x-ray computed tomography imaging^{11,12,16,17}, and two-dimensional strain mapping^{9,16} have been conducted. The development of "crush bands" within the material is observed as the material plastically deforms. This phenomenon is also observed as small oscillations in the plastic strain plateau on the stress-strain curve. Imaging techniques have also been used to correlate foam behavior to cell morphology such as cell shape and imperfections. Jagged cell walls, known as "wiggles," have been found to decrease the modulus and strength of the foam material,^{8,10} although this phenomenon is more apparent in Alporas foam than in Duocel¹⁰ foam likely due to the higher occurrence of structural imperfections in Alporas.

The growth of the experimental body of data has led to the development of several constitutive models for aluminum foams.^{13,14,18} The various models implement a range of yield criteria, strain-hardening rules and plastic-flow rules. The models rely on calibration data from uniaxial and multiaxial tests combined with traditional plasticity theory. Several of these models have been evaluated and compared by A.G. Hanssen *et al.*¹⁹ In a series of validation experiments it was shown that most all the current models accurately represent uniaxial behavior of aluminum foams, but none of them proved accurate for more complex loading modes.

Motivation

It is evident in the results of A.G. Hansen *et al.*¹⁹ that current constitutive models only accurately represent the basic loading modes for which they are calibrated. In this respect, the development of constitutive models has been hampered by a lack of experimental data under complex loading modes as well as in the post-yield regime.¹⁴ Available data for the development of constitutive models has been limited to bulk strain measurements under uniaxial, multiaxial, and hydrostatic loads.

Using digital volume correlation,^{20,25,26} full-field strains in three-dimensions have been measured under two complex loading modes into post-yield behavior in Alporas and Duocel aluminum foams. These data, and future experiments utilizing the same technique, will aid in the development of, and provide a robust validation tool for, improved constitutive models with the eventual goal of a reliable material model for consumer use in coordination with finite element packages.

Furthermore, the full-field technique outlined in this paper gives localized strain measurements in three-dimensions allowing for a completely new realm of topics to be investigated. For example, small defects which violate the continuum size assumption such as holes and notches will be critical for use of aluminum foams in structural applications, and concentration effects around such features can now be evaluated.

Strain Measurement Using Digital Volume Correlation

The digital volume correlation strain measurement technique used in this work is outlined below. For a complete description see "*Digital Volume Correlation: Three-dimensional Strain Mapping Using X-ray Tomography*" by Bay *et al.*²⁰

Digital volume correlation is an extension of two dimensional image correlation²¹ but uses three-dimensional image volumes, such as those produced by x-ray computed tomography, instead of two-dimensional surface images. Hence the first step in the process is the acquisition of high-resolution image volumes. Several techniques for acquisition of CT data exist but care must be taken to assure the resolution of the image volumes is sufficient for correlation. Critical issues include correction of two-dimensional projection images for geometric and intensity variations prior to reconstruction of the projection images into an image volume. Also, for the purposes of the reconstruction procedure, the rotation axis of the sample relative to the source and image intensifier must be determined to great accuracy. The reconstruction procedure can be carried out using a number of established algorithms depending on the type of CT system used.

Whereas two dimensional image correlation tracks unique patterns of pixels between two images to compute a two-dimensional displacement vector field, digital volume correlation tracks unique patterns of voxels (the three-dimensional analog to pixels) between an undeformed and a deformed image to compute a three dimensional displacement vector field. In the two-dimensional technique, artificial speckle patterns are commonly applied to the sample surface in order to introduce texture for correlation. In the three-dimensional technique, samples must have sufficient density variations to give distinct x-ray projection images such that unique voxel patterns will exist throughout the reconstructed image volume. The size of the voxel region tracked is variable corresponding to the texture scale of the sample and is referred to as the "subvolume."

Measurement points must be uniformly distributed throughout the sample region in order to produce a refined measurement. As the correlation proceeds, the subvolume will move to each discrete measurement point throughout the sample region in the undeformed image volume. The correlation routine calculates the displacement of a measurement point by locating the corresponding subvolume in the deformed image volume. This is accomplished by establishing an objective function (**Equation 2**) that computes the sum-of-square differences in voxel gray values between subvolumes in the two image volumes. The simplified objective function shown below accounts only for three displacement degrees of freedom, however the objective function utilized in this work also accounts for three rotational degrees of freedom. It is possible to account for strains within the subvolume (6 additional degrees of freedom), thus increasing the displacement measurement accuracy in regions of high deformation, however this has not been implemented in the current procedure.

$$C(g) = \frac{1}{2} \sum_{i=1}^w \{B(p + g + m_i) - A(p + m_i)\}^2 \quad [2]$$

Where: p is a measurement point within the measurement region,

g is a displacement vector,

m_i , a function of slice, row and column within the image volume, is an offset to a voxel location within the subvolume.

B and A are the subvolumes from the deformed and undeformed image volumes, respectively.

The equation is summed over the w points that compose each subvolume, where voxel-by-voxel comparison is controlled by m_i , thus calculating the sum-of-squared

difference between the subvolumes. The sum is computed over a user-specified range of displacement vectors, g , and the best matched displacement vector is chosen by a minimization procedure which takes place in two steps: A coarse search which directly minimizes the objective function over integer values of g within the search range, followed by a non-linear minimization technique²² incorporating an interpolation routine in order to achieve sub-voxel resolution. Completion of this procedure to compute g at all measurements points throughout the volume yields the displacement vector field.

The strain tensor field is calculated from the displacement vector field in a two step process. First, the displacement field is smoothed by fitting a polynomial to each component of the displacement vector. Next the strain field is calculated by fitting a second-order approximation of the strain tensor to a local cloud of displacement values.

EXPERIMENTAL METHODS

Equipment

In order to acquire high-resolution CT image sets under loads, a specialized system was developed under the supervision of Dr. Brian Bay with funding from the NSF through grant CMS-9977491. The details of the system are as follows: X-rays are generated by a Fein Focus FXE 160.20 cone-beam x-ray system (Fein Focus, Garbsen, Germany). Loading fixtures are mounted to Newport RV120PP rotational stages (Newport Corporation, Irvine, CA) which are permanently fixed to an Instron IN4444 load frame (Instron Corporation, Canton, Massachusetts). This combination allows for 360 degree rotation of the sample as required for CT imaging while the sample is under

load. Transmitted x-rays are captured by a Thompson TH9438HX image intensifier (Thomson Tubes Electroniques, Meudon la Foret , France), which converts x-ray energy light into the visible spectrum. This visible light is captured by a Retiga 1300 10-bit digital camera (QImaging, Burnaby, B.C. Canada) and saved in raw image format. The entire system is housed in a lead box for safety. The x-ray system, outside of the lead box, is shown below (**Figure 2**).

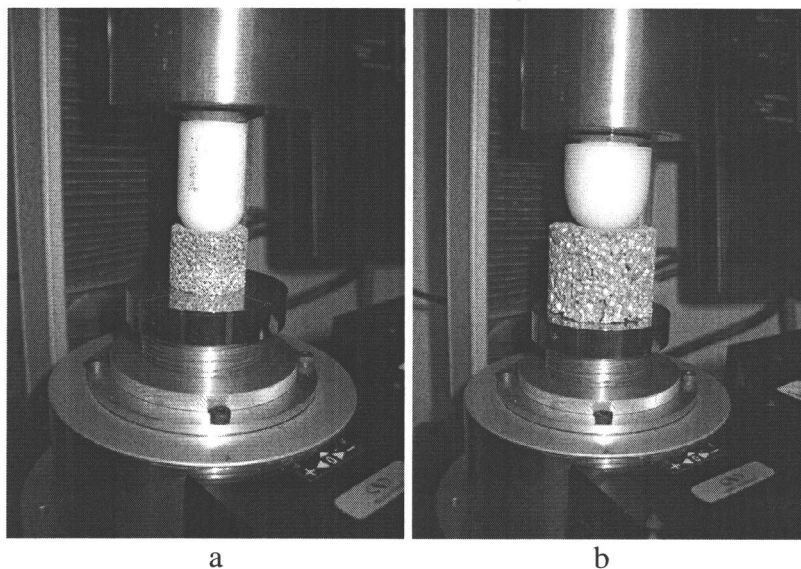


Figure 2: X-ray CT system

The acquisition process is controlled by in-house software that controls stage rotation, load frame displacement and digital camera parameters via a GPIB connection and also saves the raw projection images to a file.

Experiments

Two different experiments were conducted with open-cell Duocel foam and closed-cell Alporas foam. Two different Duocel foams were used, each with different pore sizes, and these will be referred to as "Duocel (fine)," and "Duocel (coarse)" throughout this work. In the first experiment, rigid spherical indenters were pressed into foam cylinders and the strain field below the indenters was investigated (**Figures 3a, 3b**). In the second experiment, rectangular foam samples with holes were compressed and the strain concentration in the region of the holes was measured (**Figures 3c, 3d**). Repeat scans of unloaded specimens were also taken in order to provide an estimation of experimental error.



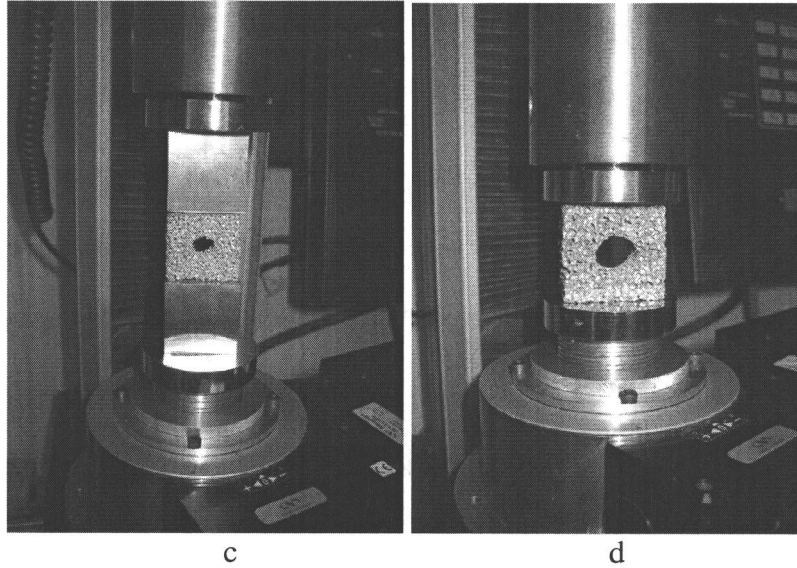


Figure 3: a) Duocel (fine) indentation b) Alporas indentation c) Duocel (coarse) with hole d) Alporas with hole

Indentation

Two cylindrical samples, one each of Alporas and Duocel (fine), were cut using a bandsaw and the flat faces were milled to be parallel. Both samples were preloaded on the flat faces to a load below the yield strength in order to flatten any burrs resulting from machining. Spherical indenters were fabricated on a lathe from Delrin plastic, which was chosen for its low x-ray attenuation. Due to the larger nominal cell size of the Alporas foam, a larger indenter was used in order to assure that size effects would not influence the strain measurements. Cylinders were placed on smooth platens and the indenters were fixed to the loading platen using a 5C collet. Indenters were lowered into the samples to three depths and CT scans were taken at zero-displacement and at each depth.

Experimental parameters are summarized below (**Table 2**).

Table 2: Indentation experiment parameters

| Sample | Duocel (fine) | Alporas |
|-----------|---------------|---------|
| Cell Type | Open | Closed |

| | | |
|---|--------------------|------------------------------|
| Porosity* | 93% | 91% |
| Mean Cell Size (mm)** | 1 ^[3] | 4.5 ^[8] |
| Sample Dimensions (mm) | r = 14.5 h = 23 | r = 23 h = 37 |
| Indenter Radius (mm) | r = 12.5 | r = 19 |
| Indentation Depths (mm) | 0.5, 1.0, 2.0 | 1.0, 2.0, 2.5, 3.0, 3.5, 4.0 |
| X-ray Intensity (kVp) | 40 | 46 |
| Exposure Time (ms) | 330 | 230 |
| Grayscale Depth | 8-bit | 10-bit |
| Reconstructed Volume Resolution (μm) | 66 | 104 |

*Measured property

**From literature

Compression with Central Hole

Two rectangular samples, one each of Alporas and Duocel (coarse), were cut using a bandsaw and the loading surfaces were milled to be parallel. Samples were preloaded below the yield strength in order to flatten any burrs that may have resulted from the machining process. In the Duocel experiment, solid aluminum blocks (38mm x 38mm x 20mm) were machined and used as loading platens in place of the standard round platens (**Figure 3c**). This was done to avoid "shadowing," which reduces the visible region of the sample, resulting from the use short samples on the wide platens with the cone-beam x-ray source. The experimental parameters are summarized below (**Table 3**).

Table 3: Compression with central hole experiment parameters

| Sample | Duocel (coarse) | Alporas |
|---------------------------------|---|--------------------|
| Cell Type | Open | Closed |
| Porosity* | 93% | 91% |
| Cell Size (mm)** | 2.0 ^[3] | 4.5 ^[8] |
| Sample Size (mm) | 36 x 36 x 10 | 45 x 45 x 19 |
| Hole Diameter (mm) | 11 | 19 |
| Displacement Levels (mm) | 0.5, 0.75, 0.95, 1.125, 1.375, 1.5, 1.625 | 0.5, 1.0, 2.0 |

| | | |
|---|-------|-------|
| X-ray Intensity (kVp) | 49 | 35 |
| Exposure Time (ms) | 200 | 229 |
| Grayscale Depth | 8-bit | 8-bit |
| Reconstructed Volume Resolution (μm) | 78 | 105 |

* Measured property

**From Literature

Repeat Unloads

In order to characterize the measurement precision, repeat CT scans of zero load cases were acquired for each of the three materials investigated. Imaging parameters for each foam were identical to those used in their respective experiments. Minimum principal strains were measured between the repeat scans. Experience has shown that the distribution of strain invariants is non-normal so non-parametric statistics were used to describe the distribution of the data. In this technique, the 17th, 50th and 83rd percentile values (representing the mean +/- one standard deviation for the non-normally distributed data) are considered to represent central tendency and variability of the data set.

Data Processing

The strain measurement procedure, as outlined in the *Strain Measurement Using Digital Volume Correlation* section above, is accomplished using a series of computer codes running on a Sun Server (Sun Microsystems Inc., Mountain View, California). See Appendix A for a flow chart outlining this process.

First, the 500 acquired projection images for each sample were corrected for both intensity and geometric variations intrinsic to the image intensifier. Intensity correction was accomplished by acquiring a "bright field" image, with no sample in place, which

gives the x-ray intensity variation across the image intensifier, and a "dark field"

image which establishes the background noise and then adjusting the projection images to correct for these effects. Geometric variations were corrected by imaging a grid of known geometry, developing an algorithm to adjust the distorted grid image to match its known geometry, and then applying the same algorithm to the projection images.

Next estimates of the rotation axes of the sample were made from the projection image data. As a first approximation, the projection images were averaged, giving an axisymmetric shape, and then an algorithm was applied to find the centroid of this shape and estimate its angle and rotation center relative to the image coordinate system. These estimates were used to reconstruct test slices from the top and bottom regions of each sample over a range of parameters. The parameters of the best-focused test slices, which were found using the Sobel edge detection routine, were chosen for the final reconstructions of the complete image volumes. All reconstructions were completed using a Feldkamp cone-beam algorithm²⁴

The displacement vector fields were calculated using the "cdi" code which takes as input two image volumes and several parameters including the subvolume size, searching range, and search technique. A subvolume size of 31 voxels³ was used in all experiments. Lastly, strains were computed from the displacements using the "gds" code through which the displacement smoothing parameters can be adjusted. See Appendix B for sample input files for the "cdi" and "gds" codes.

Strain results were visualized using MSC Patran pre- and post-processing software (MSC Software Corporation, Santa Ana, California). Three-dimensional

rendering of image volumes using T3D (Research Systems Inc., Boulder, CO) were also used for visualization.

ANALYTICAL METHODS

Compression of dense metal with central hole

A nonlinear finite element model of a dense metal (6101 aluminum) with a central hole was built in MSC Patran and solved using ABAQUS (Hibbit, Karlsson & Sorensen, Inc., Pawtucket, Rhode Island). Block dimensions were identical to those as in the Duocel compression experiment (**Table 3**). The block was meshed with 3446 10-node quadratic tetrahedron (C3D10) elements. Vertical displacement of the block was constrained at the base, however lateral expansion was allowed. A vertical displacement of 1.625 mm was applied to the top surface, as in the maximum displacement case in the Duocel experiment. An elastic, perfectly plastic constitutive model was used in order to capture the plastic strain field and provide a basis for comparison between the plastic behavior of dense metals and foams. Some manual adjustment of solution step size and allowable step number were required in order to achieve convergence.

Constitutive Modeling

A model of the indentation load scenario was built in MSC Patran for export to ABAQUS finite element software. Foam cylinders were modeled using 8-node biquadratic axisymmetric quadrilateral elements (CAX8). The indenters were modeled by specifying a circular displacement profile to the nodes in the indentation region simulating a completely rigid indenter at a depth of 3mm. Displacement of the cylinder was completely constrained along its base. The constitutive model, developed by Dr. Ronald

Miller¹³, was implemented as a user-defined subroutine for material behavior (UMAT) and specific material properties required by UMAT were specified in the ABAQUS input file. The UMAT routine depends on seven material parameters and several points from the compressive stress/strain curve. The seven parameters are:

- 1) Young's modulus
- 2) Poisson's ratio (elastic realm)
- 3) γ . Gamma is a function of the compressive yield stress, the tensile yield stress and plastic Poisson's ratio
- 4) α . Alpha is a function of Gamma (3) and plastic Poisson's ratio
- 5) ρ . Rho is the relative density, (1 - porosity), of the foam.
- 6) Sdens. The slope of the densification curve
- 7) Syield. The compressive yield stress

Typical material properties were selected based on results of previous mechanical testing^{4,8,10,12}, however the model would not converge under these parameters.

Consequently, the model was first run with parameters provided by Dr. Miller and an attempt was made to adjust parameters individually and step towards a set of parameters that better represented the aluminum foams examined in this study. As advised by Dr. Miller, first gamma and alpha parameters were adjusted independently of the other parameters to their desired values, and then other parameters were adjusted. The analytical trials are summarized below (**Table 4**) where parameters to the left of the bold line are used to evaluate γ and α but are not explicitly supplied to the UMAT subroutine. Trial one used the parameters supplied by Dr. Miller and trials six and eight were the desired parameter sets for the Alporas and Duocel foams respectively.

Table 4: Parameters supplied to UMAT subroutine

| Trial | σ_c | σ_t | v_{pl} | E | ν | γ | α | ρ | Sdens | Syield | Converge |
|--------------|------------|------------|----------|----------|-------|----------|----------|--------|--------------|---------------|-----------------|
| 1 | 1.3 | 1.7 | 0 | 240 | 0.33 | -0.5467 | 1.918 | 0.08 | 200 | 1.0 | Yes |
| 2 | 1.3 | 1.7 | 0 | 240 | 0.33 | -0.5467 | 1.918 | 0.08 | 200 | 1.3 | No |
| 3 | 1.3 | 1.7 | 0.024 | 240 | 0.33 | -0.5326 | 1.708 | 0.08 | 200 | 1.0 | Yes |
| 4 | 1.3 | 1.7 | 0.024 | 500 | 0.33 | -0.5326 | 1.708 | 0.08 | 200 | 1.0 | Yes |
| 5 | 1.3 | 1.7 | 0.024 | 500 | 0.33 | -0.5326 | 1.708 | 0.08 | 500 | 1.0 | Yes |
| 6 | 1.3 | 1.7 | 0.024 | 500 | 0.33 | -0.5326 | 1.708 | 0.08 | 500 | 1.3 | No |
| 7 | 1.3 | 1.9 | 0.052 | 500 | 0.33 | -0.6966 | 1.158 | 0.08 | 500 | 1.0 | No |
| 8 | 1.3 | 1.9 | 0.052 | 500 | 0.33 | -0.6966 | 1.158 | 0.08 | 500 | 1.3 | No |

RESULTS

Experimental

X-ray CT imaging data of sufficient resolution for the digital volume correlation measurement technique was collected for three different aluminum foams. Displacements and strains were successfully measured under load in indentation and uniaxial compression experiments. Some complications resulted from the large displacement and crushing in the indentation experiments, but these were resolved using an incremental correlation technique. In this technique, displacement measurements at small load steps were used as starting points for tracking the deeper and more deformed subvolumes at higher load steps. Incremental analysis was not required for the uniaxial compression experiments.

Results for the two experiments, the characterization of error, and the analytical modeling are shown. In all cases, minimum principal strains are reported since they provide a good indication of strain behavior in the compressive loading mode.

Indentation

Results of the Duocel (fine) and Alporas cylindrical samples are shown on the following two pages (**Figures 4,5**). The left column shows renderings of rectangular regions below the indenter from the reconstruction volume data. The right column shows fringe plots of minimum principal strain values superimposed on the deformed shape of the indented cylinders which have been sliced through a diametrical plane to reveal the strain field directly below the indenter. Peak minimum principal strain values of 39.7% and 22.3% were measured in the Duocel and Alporas respectively. A clear difference in the depth of the highest strain field was observed between the open and closed cell foams (**Figures 4,5**). This difference has been quantitatively analyzed (**Figure 6**) where the depth of peak strain and the depth of indentation have been scaled to sample height for the purposes of comparison.

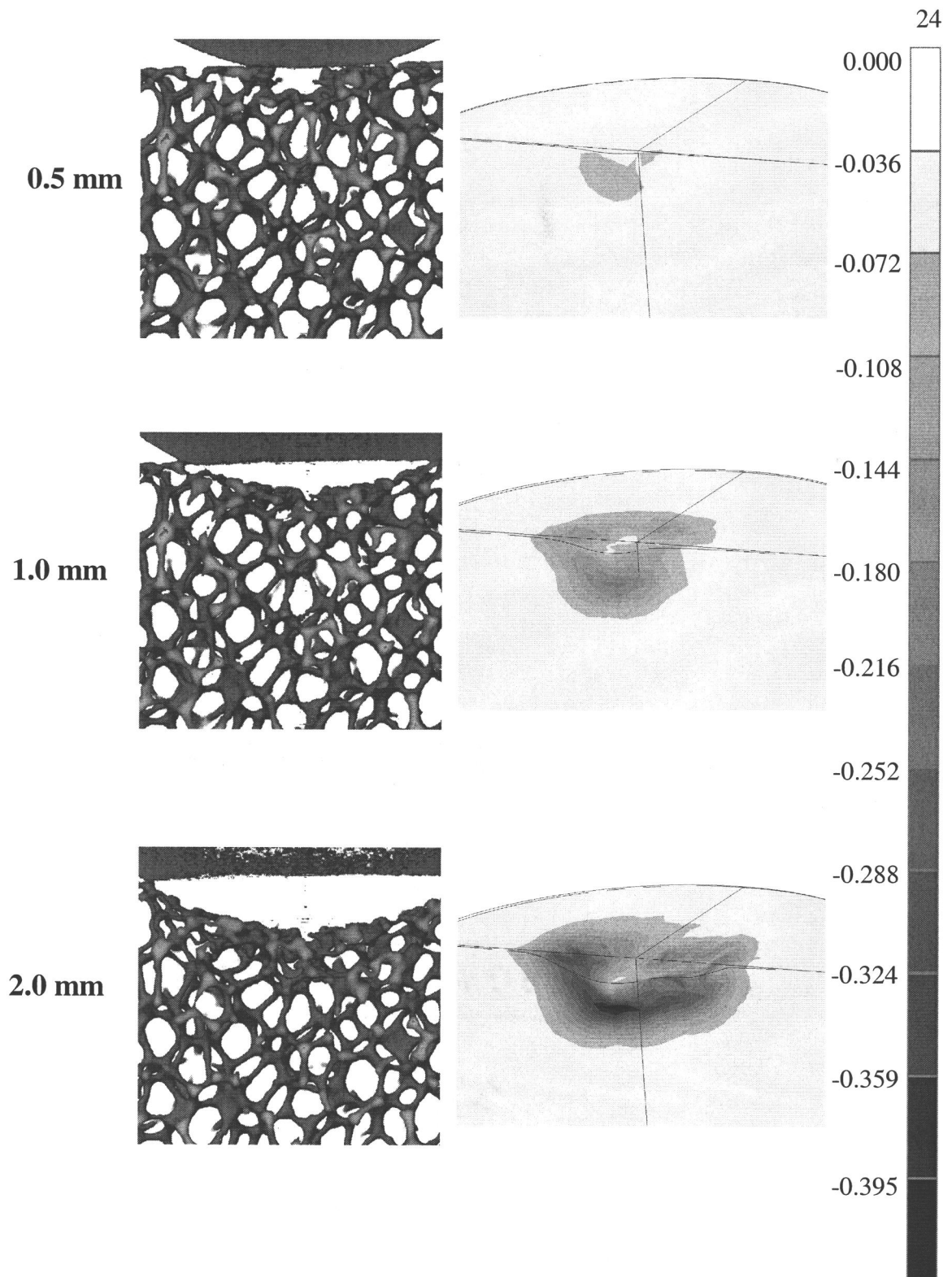


Figure 4: Minimum principal strains on a diametrical plane in Duocel (fine) foam under indentation loading with corresponding renderings

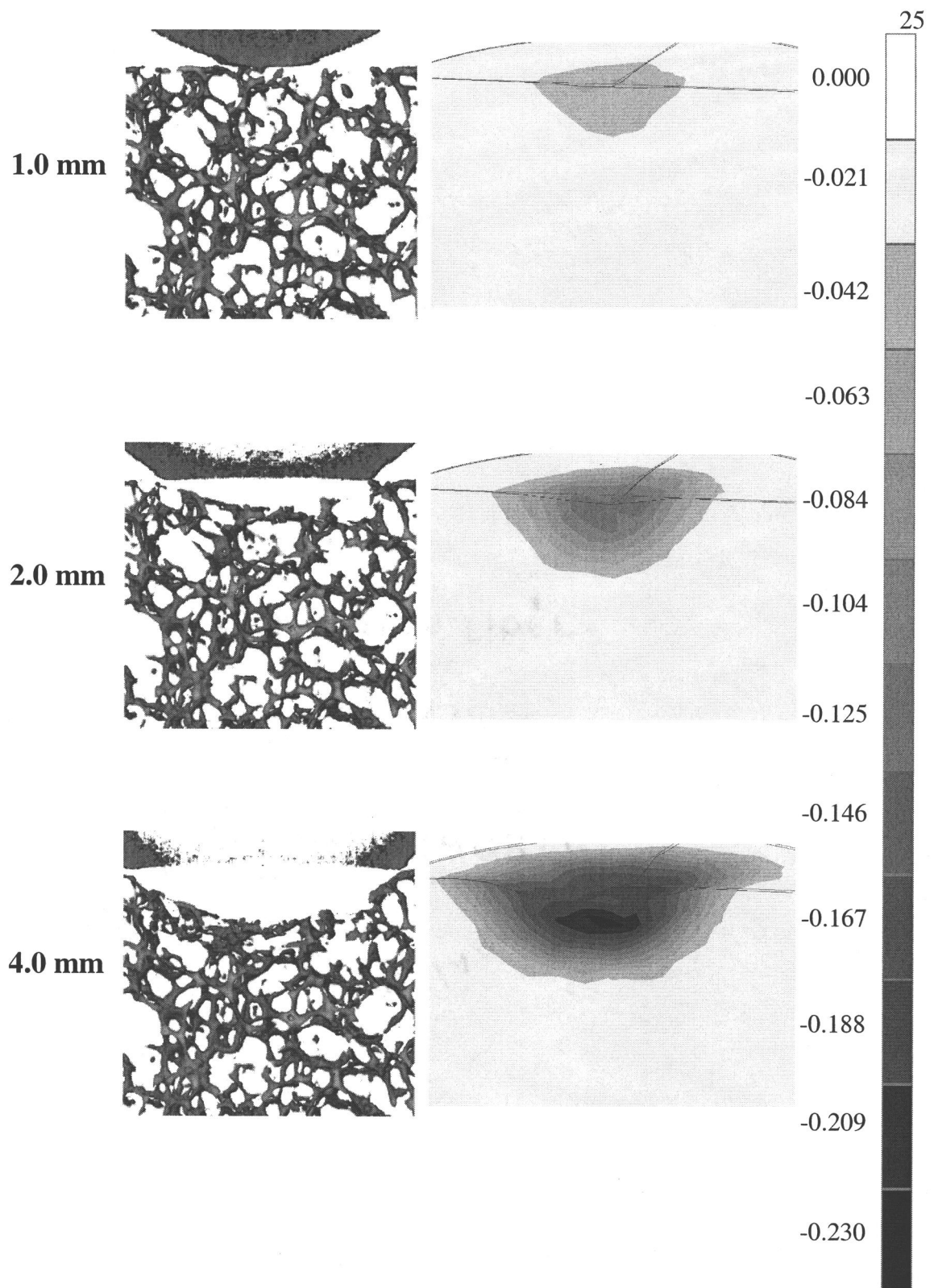


Figure 5: Minimum principal strains on a diametrical plane in Alporas foam under indentation loading with corresponding renderings

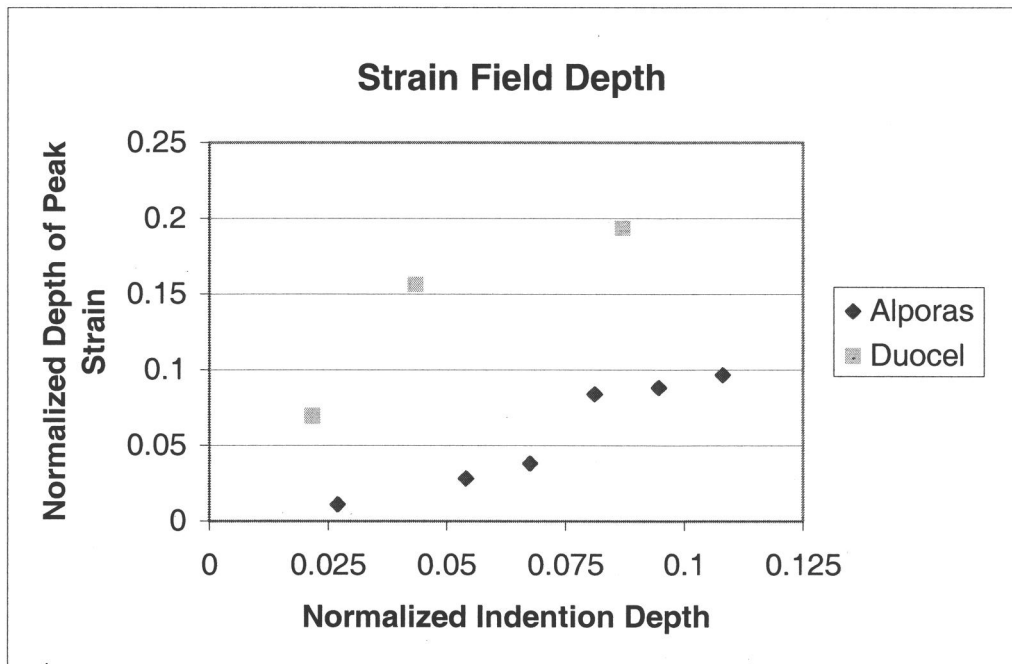


Figure 6: Comparison of strain field depth between Alporas and Duocel (fine)

Compression with Central Hole

Results of the compression experiments are shown (**Figures 7,8,9**) for Duocel (coarse) and Alporas samples with central holes. The left column of each figure shows renderings of the reconstructed image volume data. The rendering of the Alporas sample has been cropped slightly, in a plane normal to the image, to reveal cell structure. The right column of the images shows minimum principal strain fringe plots superimposed onto the deformed sample shape. Greatest principal strain values of 16.6% and 32.8% were measured for the Duocel and Alporas respectively.

Qualitative observation of both projection images and renderings showed similar patterns of failure for both foams. Initial failure occurred along a horizontal band on one side of the hole (**Figure 7 left**). The length reduction in the side of initial failure caused a corresponding strain concentration on the inner hole surface on the opposite side (**Figure**

8). In the Duocel experiment, the foam was compressed further until secondary failure²⁷ along a plane oriented approximately 50 degrees from horizontal was observed (**Figure 7 right**).

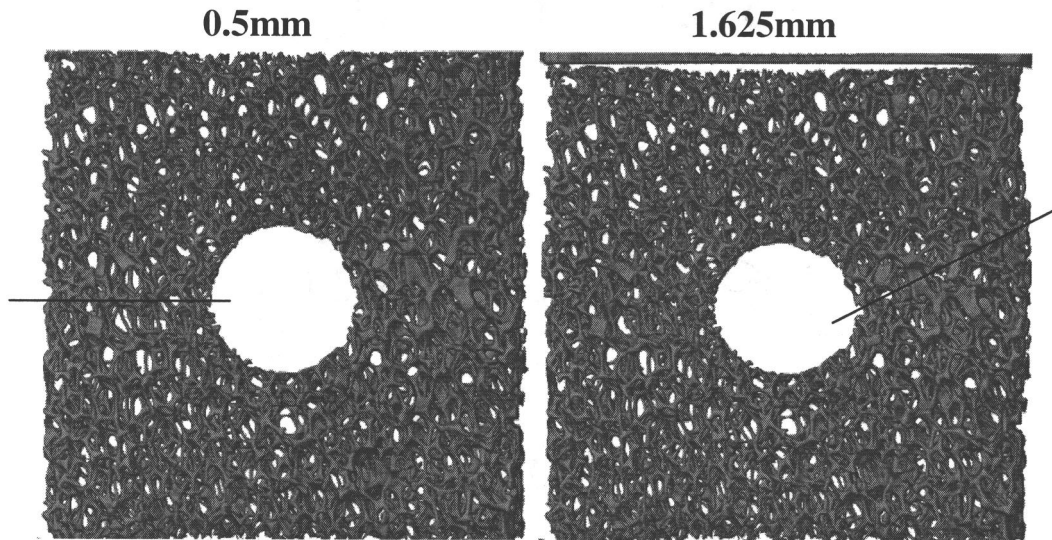


Figure 7: Approximate planes of initial (left) and secondary (right) failure in Duocel (coarse) foam

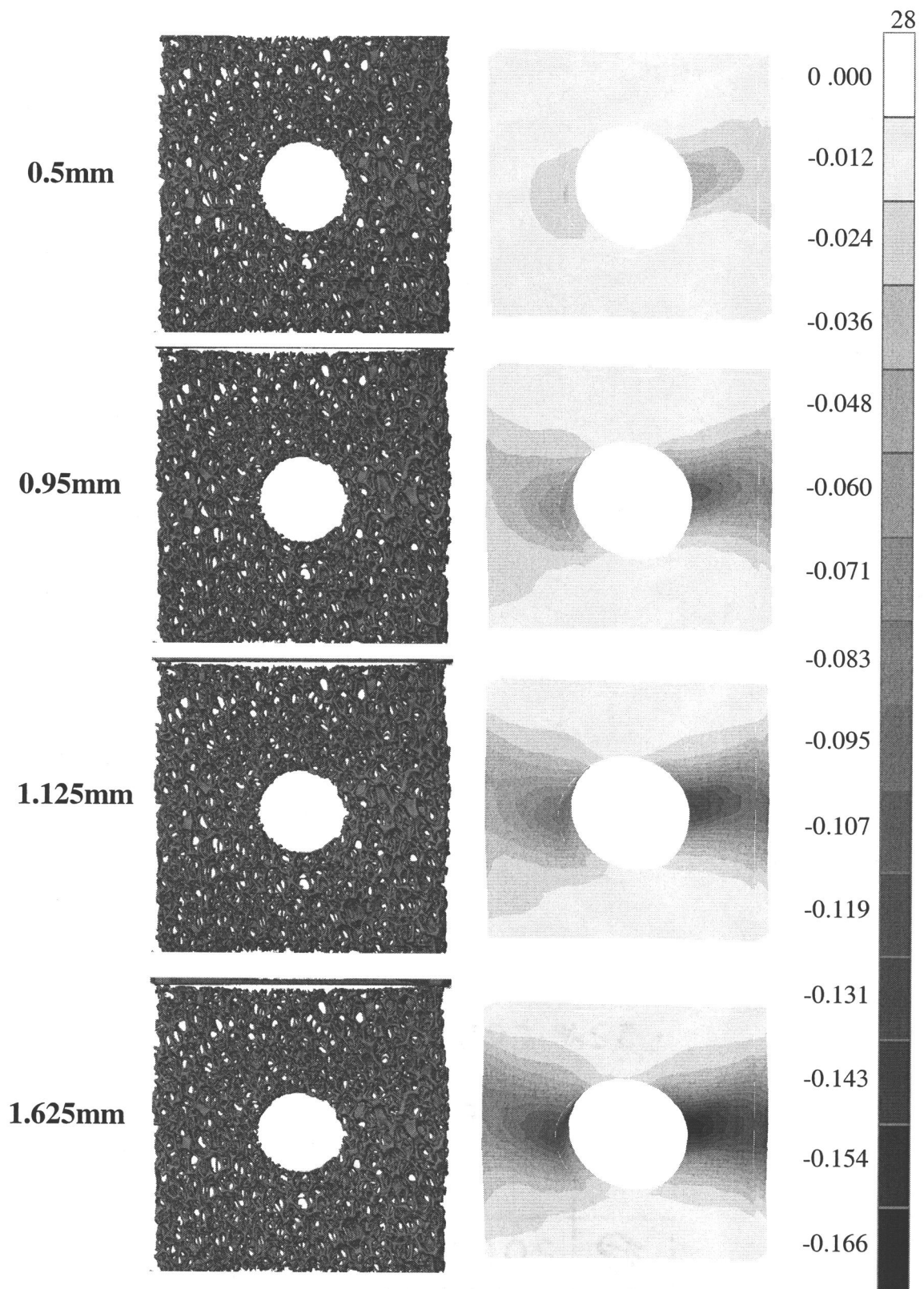


Figure 8: Minimum principal strains in Duocel (coarse) foam under uniaxial compressive loading with corresponding renderings

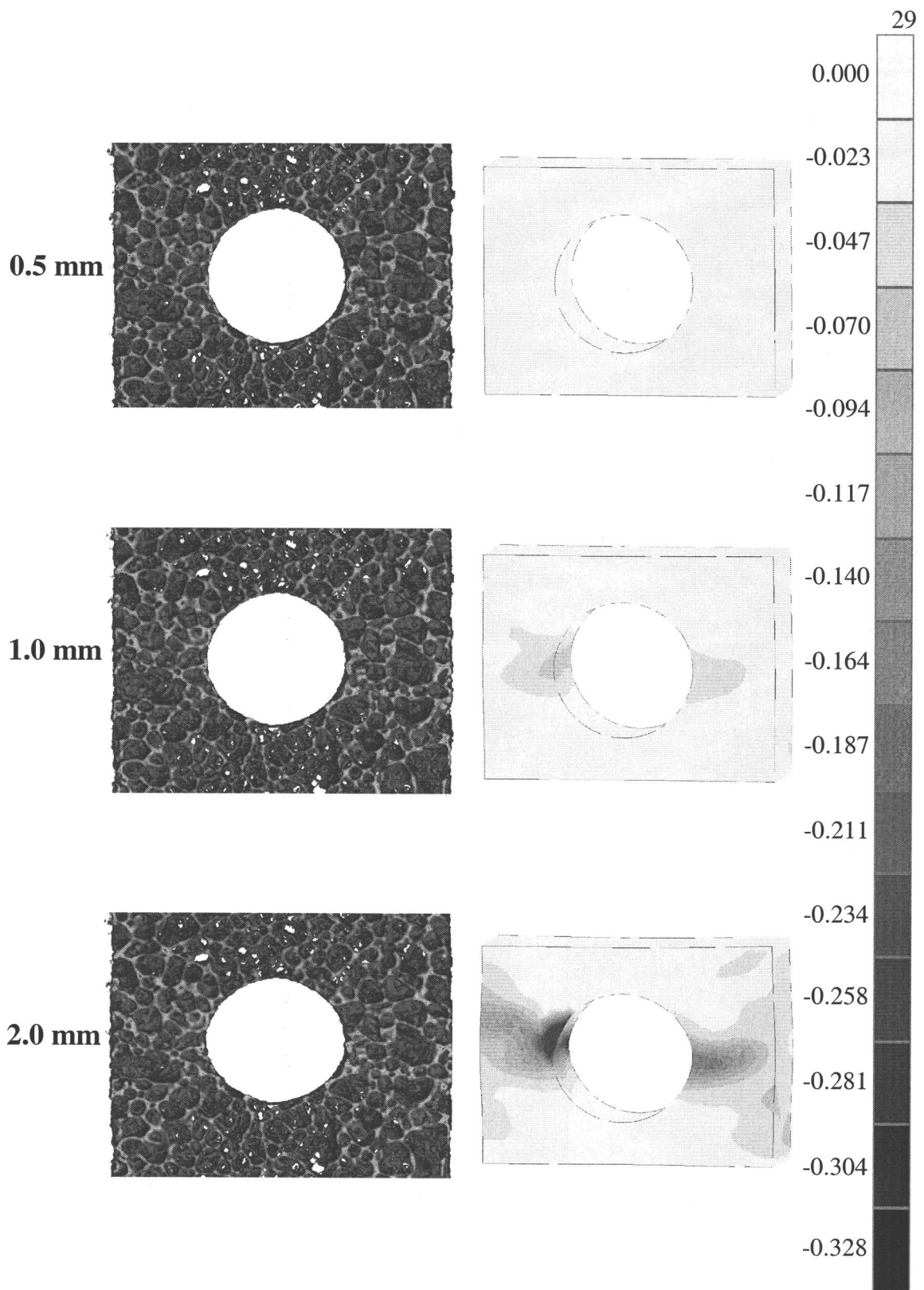


Figure 9: Minimum principal strains in Alporas foam under uniaxial compressive loading with corresponding renderings

Repeat Unloads

Characterization of measurement precision was established for the three materials examined in this work through the repeat unload experiments. The measured values of minimum principal strains in each of the unloaded samples is shown (**Figures 10, 11, 12**).

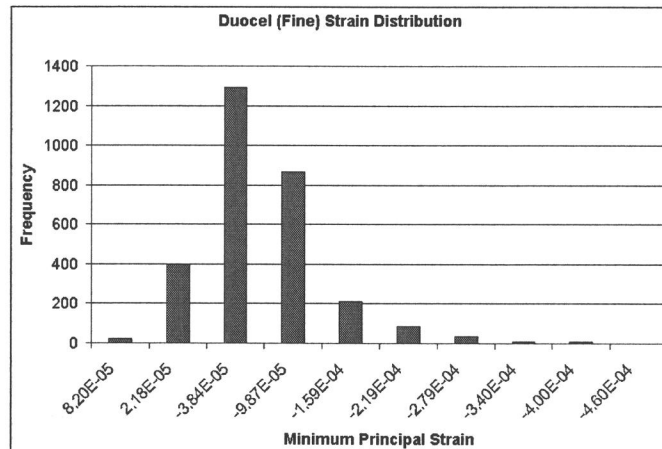


Figure 10: Minimum principal strain distribution in Duocel (fine) repeat unload experiment

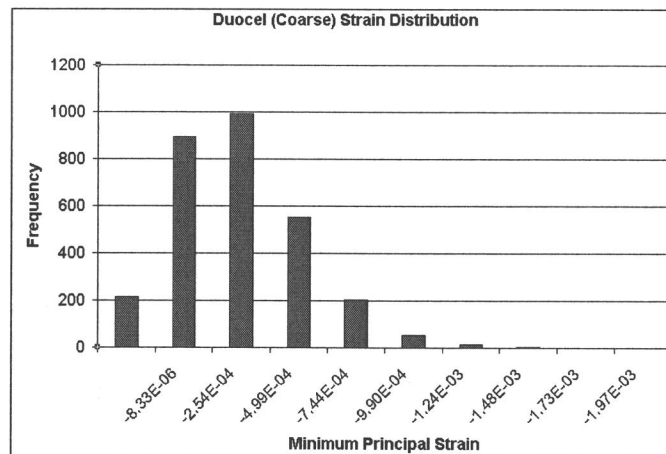


Figure 11: Minimum principal strain distribution in Duocel (Coarse) repeat unload experiment

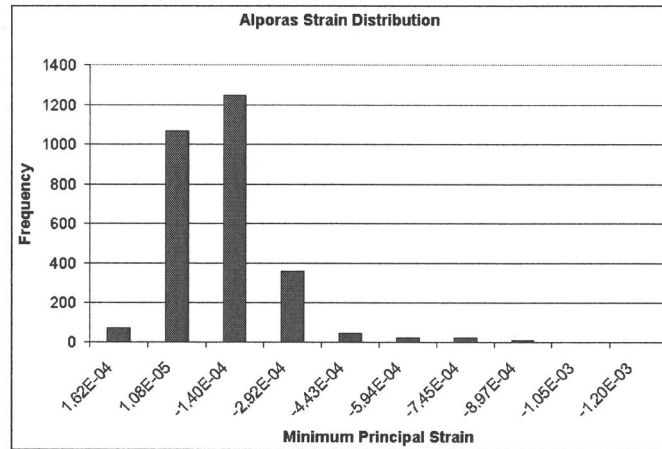


Figure 12: Minimum principal strain distribution in Alporas repeat unload experiment

Strain distributions were not normally distributed so non-parametric descriptive statistics were used to represent the data (**Table 5**). Comparison of peak measurement-noise values to peak measured strain values from the indentation and compression experiments shows that error values are approximately 0.1-1.2% of measured values.

Table 5: Representative minimum principal strain values from repeat unload experiments

| Material | 17 th Percentile | 50 th Percentile | 83 rd Percentile | Peak Value |
|-----------------|-----------------------------|-----------------------------|-----------------------------|------------------------|
| Duocel (Fine) | -1.392×10^{-4} | -9.00×10^{-5} | -4.40×10^{-5} | -4.64×10^{-4} |
| Duocel (Coarse) | -6.190×10^{-4} | -3.32×10^{-4} | -1.08×10^{-4} | -1.97×10^{-3} |
| Alporas | -2.880×10^{-4} | -1.67×10^{-4} | -7.30×10^{-5} | -1.20×10^{-3} |

Analytical Models

Compression of Dense Metal with Central Hole

A peak minimum principal strain value of 43.6% was calculated for an applied vertical displacement of 1.625mm on the top surface of the block. The strain field was much more uniform than in the experimental result with planes of high strain oriented at approximately 45 degrees (**Figure 13**). The deformed shape shows significant Poisson expansion, which is contrary to the experimental foam results, as expected.

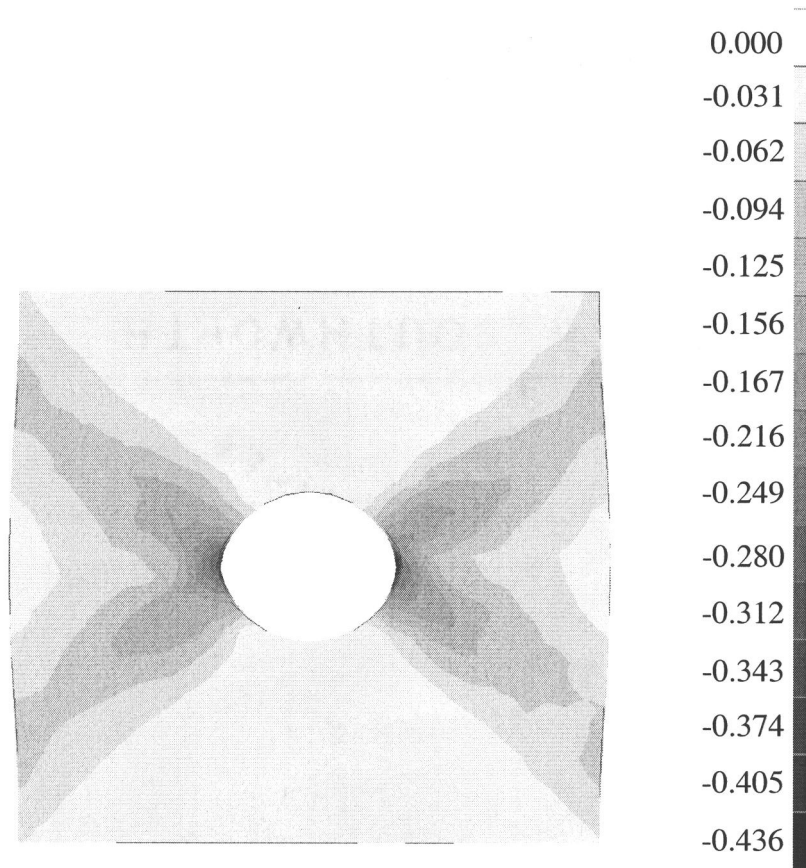


Figure 13: Minimum principal strains in a dense metal finite element model

Constitutive Modeling

The peak minimum principal strain values for each of the analytical trials (**Table 4**) are shown (**Table 6**).

Table 6: Results of Constitutive Model Trials

| Trial | Converge | Peak Minimum Principal Strain |
|--------------|-----------------|--------------------------------------|
| 1 | Yes | 0.899 |
| 2 | No | N/A |
| 3 | Yes | 0.890 |
| 4 | Yes | 0.916 |
| 5 | Yes | 0.916 |
| 6 | No | N/A |

| | | |
|---|----|-----|
| 7 | No | N/A |
| 8 | No | N/A |

Observed strain fields were shallow to the indenter as compared to the experimental results (**Figure 9**), no qualitative difference is evident in the strain field between the trials, and no substantial quantitative difference in peak strain was observed (**Table 6**). The magnitude of the analytical strain values is approximately four times that of the experimentally measured values for Alporas foam.

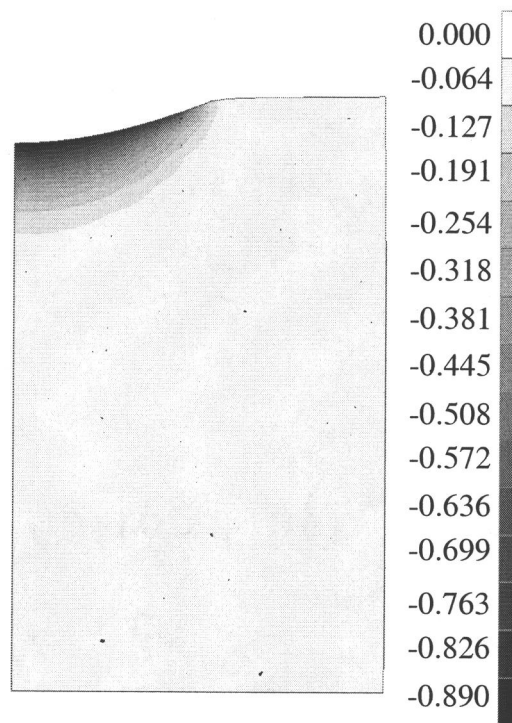


Figure 14: Minimum principal strain in axisymmetric indentation model

The parameter set of trial five was an accurate representation of the material properties of the Alporas foam used in the experimental measurements with the exception of the "Syield" parameter. The model was very sensitive to adjustment of this parameter and only the original value of 1.0 would allow the model to converge. This created an

inconsistency between the compressive yield value used to calculate the γ and α parameters and the "Syield" parameter. Trial seven showed that model convergence was also sensitive to changes in γ and α and consequently analytical results could not be obtained for a parameter set representing Duocel foam.

DISCUSSION

Indentation

The indentation experiment showed a difference in the depth of the highest strain region between the Alporas and Duocel foams. From the renderings of the image volumes it is evident that deformation is transferred deeper into the Duocel than the Alporas. A possible reason for this difference is the cell morphologies of the two foams. Duocel is composed mostly of struts that are roughly circular in cross-section. When these struts are aligned approximately parallel to the direction of indentation, force is transmitted along their long-axes, and deformation is transferred deep into the sample. At junctions where these axially loaded struts meet perpendicularly, or at a steep angle to another strut, buckling occurs. Conversely, Alporas foam is composed of spherical cells with thin walls. At the surface of the Alporas sample where these spheres are cut, thin vertical walls are exposed and these thin walls are highly susceptible to buckling. For deep deformation to occur in Alporas, first the top layer of incomplete spheres must be completely crushed and densified. This process is evident in the "indentation depth versus strain depth" comparison (**Figure 4**) where there is a substantial increase in the strain field depth between the third and fourth load step. Due to the closed-nature of Alporas

foam, renderings of the deformed Alporas are not as informative as those of the Duocel samples.

From initial images of the Alporas foam, the mean cell size was estimated to be approximately 2 mm, twice that of the Duocel (fine) foam. Based on this estimation, an effort was made to scale the Alporas indentation experiment parameters by a factor of two, relative to the Duocel experiment, in order to both assure size effects did not distort the results and to provide a uniform basis for comparison. Subsequent literature searches revealed that the mean cell size was approximately 4.5 times that of Duocel (fine) foam. Consequently the indenter size used in the Alporas indentation was small enough such that size effects may have affected the results. It is possible that a larger indenter would reduce the degree of localized crushing and the strain field would be transmitted deeper into the Alporas sample at a lesser indentation depth.

Compression with Central Hole

Contrary to the indentation experiment, the Alporas and Duocel foams with a central hole behaved similarly under compressive loading. As outlined in the results section, both exhibited a pattern of failure where one side crushed in a uniform horizontal band followed by failure along an angled plane in the second side. This is distinctly different than the dense aluminum finite element results where crushing does not occur and high strain regions lie along two planes oriented at approximately 45 degrees relative to the horizontal. The region of high strain is concentrated at the inside edge of the hole in the dense metal result whereas in the foam specimens, the highest strain region is distributed across the entire crushed region. The deformed shapes of the samples show

the significant difference in Poisson expansion between dense metals and foams. From the rendered foam images, the distortion appears to be a result of slipping along the 50-degree failure plane rather than a Poisson effect.

The compression experiments, particularly the Alporas sample, measure strain in specimens where the holes are small enough such that size effects alter the strain field. An understanding of foam behavior around small features such as holes will be critical to bringing aluminum foams to widespread use in structural applications. Uniaxial and biaxial testing provide sufficient knowledge for applications such as energy absorbing crash boxes, but a deeper understanding must be gained in order for these materials to be used confidently in applications such as aircraft bodies where concentration effects around fasteners are of great importance. It is possible that constitutive models will eventually be able to predict these effects, but at the present, digital volume correlation is the best source of full-field three-dimensional strain data and rigorous experimental application of this technique could build a database of information relevant to more complex applications of aluminum foams.

Repeat Unloads

Strain measurement on repeat scans of unloads provided a characterization of the effect of image of quality and processing on the final strain measurement. These results should not be taken as direct error in the measurements. In the absence of a second established measurement technique for these materials which would provide a direct error measurement, these results are useful in evaluating the magnitudes of experimental strain results compared to the magnitudes of strains resulting from background noise. The ratio

of the peak values of experimentally measured strain compared to peak background noise is low, ranging from 0.1% to 1.2%. Considering the 17th to 83rd percentile range of strains (representing the mean +/- one standard deviation for the non-normally distributed data) in the repeat unloads reduces the ratio to a range of 0.01% to 0.07%.

Of the three materials considered, the Duocel (fine) material produced the lowest level of background strain level between unloaded scans. Throughout the experiments, a consistent subvolume size was used, 15 voxels. Due to the smaller cell size of the Duocel (fine) material, more distinct features (e.g. struts) are present in each subvolume than in the case of the other two materials. The uniqueness of these subvolumes increases the precision of the strain correlation procedure, which results in lower strain magnitudes when comparing identical unloaded samples. This suggests that larger subvolumes may have increased the measurement precision in the Alporas and Duocel (coarse) samples.

Constitutive Modeling

Convergence of the constitutive model was very sensitive to input parameters. Consequently, it was difficult to adjust the parameter set to correspond with the experimentally tested materials, although a parameter set which nearly approximated the experimentally measured Alporas foam was implemented successfully. Throughout the process of adjusting individual parameters, four different strain results were produced, and these results were consistent in magnitude and strain field distribution despite the varying input parameters. Furthermore, the analytical magnitudes were approximately four times the measured strains and the strain field was much more concentrated near the indenter than in the experimental result.

Constitutive modeling implemented through finite element analysis has the potential to allow for computer-aided design of sophisticated metallic foam structures where an understanding of complex stress states is paramount. The ability to predict foam behavior without the use of costly equipment such as the x-ray imaging hardware used in this experiment will be a catalyst in the implementation of metallic foam in a wide range of applications. Unfortunately, metallic foam constitutive models have thus far been limited to the accurate prediction of relatively simple stress states such as uniaxial and biaxial loading, likely in part because experimental data has also been limited to these realms. The experimental results obtained in this work provide the first three-dimensional measurement of strain in aluminum foams under complex loading states and present a powerful development and validation tool for the creation of more accurate constitutive models.

An important feature of constitutive models when considering their eventual use in an industrial setting is the parameter set required by the model. The model in this experiment required seven parameters that could be obtained relatively easily using a uniaxial testing system and an extensometer. However, using these parameters the model was unable to predict complex strain fields such as those produced by indentation. In order for a constitutive model to be successful, its parameter set must be small enough for practical measurement yet large enough to accurately predict complex behavior. For example, the differences between trials 6 (Alporas representation) and trial 8 (Duocel representation) (**Table 4**) in terms of the parameters supplied to the constitutive model are very subtle, but the resulting strain field distributions are substantially different as

shown in the indentation experiment result. This suggests that additional parameters are likely required for the model to differentiate between the Duocel and Alporas foams.

Future Work

In order to provide better data in the indentation experiment, the experiment should be repeated using an indenter with a radius of at least 29 mm in order to assure that size effects do not distort the results. Measurements on multiple samples to confirm the differences in behavior between the foams, and perhaps even development of a database of results for various foams, would be beneficial.

In the evaluation of small features, such as holes, an experiment evaluating strain distributions due to holes of varying size and under compression, tension and shear would be of immediate benefit for design purposes.

The results of the strain measurement on unloaded samples shows that subvolume size can have a significant effect on the magnitude of background noise. In future experiments, initial correlation of unloaded specimens as a first step would establish the best subvolume size for future experiments carried out with a given material.

The experimental results obtained here could be of substantial benefit to the development of constitutive models and a close collaboration with modelers would accelerate model development.

CONCLUSIONS

- High resolution three-dimensional image volumes were acquired under load using a unique x-ray computed tomography system

- Digital volume correlation was successfully used to measure full field strains in three dimensions for three different aluminum foams under two different loading schemes
- Strains were transmitted deeper into Duocel open-cell foam than Alporas closed-cell foam under indentation loading
- Deformation and strain behavior of Alporas and Duocel blocks with a central hole under uniaxial compression was similar
- The constitutive model developed by Dr. Miller is very limited in adjustability and therefore is not suitable for modeling a range of different aluminum foams
- When provided a parameter set that approximates the material parameters of Alporas foam, the constitutive model developed by Dr. Miller does not accurately represent the behavior of Alporas under indentation loading

BIBLIOGRAPHY

- ¹Banhart, J., "Manufacture, characterization and application of cellular metals and metal foams," *Progress in Materials Science*, **46**, 559-632 (2001)
- ²Miyoshi, T., Itoh, M., Akiyama, S., Kitahara, A., "Aluminum Foam, "Alporas": The Production Process, Properties and Applications" Materials Research Society Symposium, Porous and Cellular Materials for Structural Applications, **521**, 133-137 (1998)
- ³ERG Materials and Aerospace Corporation, "Duocel Aluminum Foam" <http://ergaerospace.com/duocel.pdf>, accessed 4/17/2003
- ⁴Ashby, M.F., Evans, A., Fleck, N.A., Gibson, L.J., Hutchinson, J.W., Wadley, H.N.G., *Metal Foams: A Design Guide*, Butterworth-Heinmann, Boston, MA, 2000
- ⁵Andrews, E.W., Gioux, G., Onck, P., Gibson, L.J., "Size effects in ductile cellular solids. Part II: experimental results," *International Journal of Mechanical Sciences*, **43**, 701-713 (2001)
- ⁶Ashby M.F., Gibson, L.J., *Cellular Solids: Structure and Properties*, Cambridge University Press, Cambridge, United Kingdom, 1997
- ⁷San Marchi, C., Mortensen, A., "Deformation of Open-Cell Aluminum Foam," *Acta Materialia*, **49**, 3959-3969 (2001)
- ⁸Sugimura, Y., Meyer, J., He, M.Y., Bart-Smith, H., Grenstedt, J., and Evans, A.G., "On the Mechanical Performance of Closed Cell Al Alloy Foams," *Acta Materialia*, **45**, 5245-5259 (1997)
- ⁹Motz, C., Phipps, R., "Deformation Behaviour of Closed-Cell Aluminum Foams in Tension," *Acta Materialia*, **49**, 2463-2470 (2001)
- ¹⁰Andrews, E., Sanders, W., Gibson, L.J., "Compressive and tensile behaviour of aluminum foams," *Materials Science and Engineering*, **A270**, 113-124 (1998)
- ¹¹McCullough, K.Y.G., Fleck, N.A., and Ashby, M.F., "Uniaxial Stress-Strain Behaviour of Alloy Foams," *Acta Materialia*, **47**, 2323-2330 (1999)
- ¹²Gioux, G., McCormack, T.M., Gibson, L.J., "Failure of aluminum foams under multi-axial loads," *International Journal of Mechanical Sciences*, **42**, 1097-1117 (2000)
- ¹³Miller, R.E., "A continuum plasticity model for the constitutive and indentation behaviour of foamed metals," *International Journal of Mechanical Sciences*, **42**, 729-754 (2000)
- ¹⁴Desponded, V.S., Fleck, N.A., "Isotropic constitutive models for metallic foams," *Journal of the Mechanics and Physics of Solids*, **48**, 1253-1283 (2000)
- ¹⁵Simone, A.E., Gibson, L.G., "Aluminum Foams Produced by Liquid-State Processes," *Acta Materialia*, **46**, 3109-3123 (1998)
- ¹⁶Bustards, A.F., Bart-Smith, H., Evans, A.G., "Experimental analysis of deformation mechanisms in a closed-cell aluminum alloy foam," *Journal of the Mechanics and Physics of Solids*, **48**, 301-322 (2000)
- ¹⁷Bart-Smith, H., Bustards, A.F., Mum, D.R., Evans, A.G., Speck, D.J., Wadley, H.N.G., "Compressive Deformation and Yielding Mechanisms in Cellular Al Alloys Determined Using X-ray Tomography and Surface Strain Mapping," *Acta Mater.*, **46**, 3583-3592 (1998)

- ¹⁸Schreyer, H.L., Zuo, Q.H., Maji, A.K., *"Anisotropic Plasticity Model for Foams and Honeycombs,"* Journal of Engineering Mechanics, **120**, 1913-1930 (1994)
- ¹⁹Hanssen, A.G., Hopperstad, O.S., Langseth, M., Ilstad, H., *"Validation of constitutive models applicable to aluminum foams,"* International Journal of Mechanical Sciences, **44**, 359-406 (2002)
- ²⁰Bay, B.K., Smith, T.S., Fyhrie, D.P., Saad, M., *"Digital Volume Correlation: Three-dimensional Strain Mapping Using X-ray Tomography,"* Experimental Mechanics, **39**, 218-227 (1999)
- ²¹Chu, T.C., Ranson, W.F., Sutton, M.A., Peters, W.H., *"Applications of Digital-Image-Correlation Techniques to Experimental Mechanics,"* Experimental Mechanics, **25**, 232-244 (1985)
- ²²Gill, P.E., Murray, W., Wright, M.H., *Practical Optimization*, Academic Press, London, (1981)
- ²³Geers, M.G.D., De Borst, R., Brekelmans, W.A.M., *"Computing Strain Fields From Discrete Displacement Fields In 2D-Solids,"* International Journal of Solid Structures, **33**, 4293-4307 (1996)
- ²⁴Feldkamp, L.A. m Davis, L.C, Kress, J.W., *"Practical Cone-beam Algorithm,"* Journal of the Optical Society of America, **1**, 612-619 (1984)
- ²⁵Smith, T.S., Bay, B.K., *"Experimental Measurement of Strains using Digital Volume Correlation,"* ASTM Special Technical Publication, n 1402, p 117-126, 2001.
- ²⁶Smith, T.S., Bay, B.K., Rashid, M.M. *"Digital Volume Correlation Including Rotational Degrees of Freedom During Minimization",* Experimental Mechanics, **42**, 272-278 (2002)

APPENDICES

Appendix A: Data Processing and Analysis Procedure

A flow chart outlining the experimental procedure is shown (**Figure 13**). Data set sizes are given for a nominal data set however actual sizes may vary depending on image cropping and resolution parameters defined in the various parameter input files.

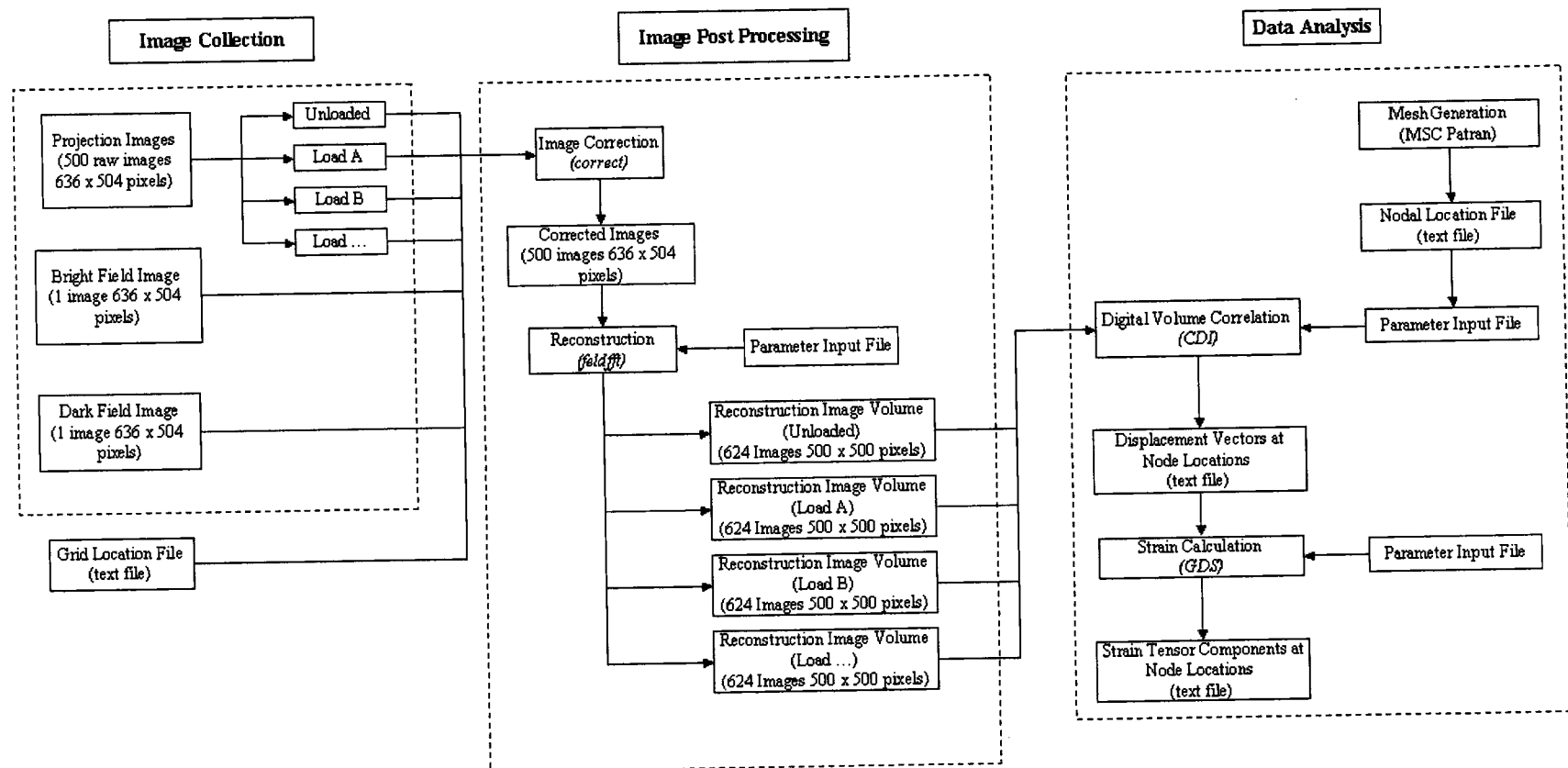


Figure A1: Flow chart of experimental procedure

Appendix B: Sample input files

Input files for the reconstruction (feldfft), displacement measurement (cdi), and strain calculation (gds) procedures are shown. The particular files below are from the uniaxial compression with hole experiment on Duocel (coarse) foam.

Feldfft input file:

```
#####
#           Input file for cone beam reconstruction           #
#####

#####
# Scanner geometric parameters      #
# Distances is mm, angles in deg   #
#####

rotation_direction      -1

source-to-detector      760.0
source-to-rotation      240

axis_tilt(alpha) 0.5
axis_tilt(beta)   0.5

#####
# Reconstruction space description                                     #
#                                                                     #
# reconstruction_region options: NOMINAL, CROPPED                   #
#                                                                     #
# NOMINAL = voxel space matches entire projection                  #
# CROPPED = voxel space matches a projection sub-region            #
#                                                                     #
# for NOMINAL, specify x_num_vox                                    #
#                                                                     #
# for CROPPED, specify x_num_vox, u_min, u_max, v_min, v_max      #
#                                                                     #
#####

reconstruction_region    CROPPED

x_num_vox    500

u_min        0
u_max        503

v_min        0
v_max        635
```

```
#####
# Detector description                                     #
# Size is the effective size of the detector, in mm      #
# Centers are real, in pixel coordinates                 #
# The (row,col) size of the images is read from the image file #
#####
```

```
u_detect_size      123.89
v_detect_size      154.86
```

```
u_detector_center_location  252.00
v_detector_center_location  318.00
```

```
u_rotation_center_location  258.86
v_rotation_center_location  318.00
```

```
#####
# Filtering parameters                                     #
# Options: RAM_LAK, SHEPP_LOGAN                           #
#####
```

```
filter_type RAM_LAK
histogram_trim 0.001
```

```
#####
# Filtering parameters                                     #
# Options: RAM_LAK, SHEPP_LOGAN                           #
#####
```

```
centering          OFF
```

```
range_resolution(u_center)          1.0    5
```

```
range_resolution(alpha)             0.25   5
```

```
range_resolution(beta)              0.50   5
```

```
slice_location_1      261
```

```
#####
#
#               cdi.3d input file
#
#####

source_CT_filename      ../050mm/ocfoam-050-r1.CT
target_CT_filename      ../100mm/ocfoam-100-r1.CT
p3neutral_filename      mesh2.out
cdioutput_filename      050mm-100mm.cdi
number_of_srch_dof      6                ### 3 or 6
objective_function      sumofsquares      ### sumofsquares,
normalized
interpolation_type      trilinear         ### trilinear,
cubic_diff, cubic_half
coarse_search_mthd      rolldownhill     ### rolldownhill, globalsearch
detail_search_mthd      bfgs             ### powell, levenberg,
bfgs, steepest
start_pnt_estimate      nearest          ### constant, nearest
disp_ref_method         total            ### total, increment
gray_thresh 75
mask_size 20
mask_skip 1
range_size 10
range_skip 3
start_and_number        1      0
global_start_vect       0      0      0      0      0      0

#####
#
#               usage notes
#
#####

### number_of_srch_dof 3 is displacement only
```



```
### number_of_srch_dof 6 is displacement plus rotation

### for number_of_srch_dof 6, use detail_search_mthd bfgs

### for disp_ref_method increment:
###   -> add disp_ref_filename      filename
###   -> add total_disp_limit

### gray values between gray_thresh and 255 are included in the
analysis

### do find all points, use node_start_number 1 0

### specify number_of_srch_dof values for global_start_vect
```

```
# The number of spatial dimensions (use 3 only)
nsd 3

# Name of the neutral file.
mesh2.out

# Output file name
050mm-100mm.gds

# Number of target files.
ndis 1

# Name(s) of the target file(s).
050mm-100mm.cdi

# Type of smoothing to do
smooth svd

# Number of points to use for smoothing
fspan 60

# Number of singular values to keep.
numsv 6

# Number of points to use for Tensor fit.
Kspan 60
```